Available online at www.sciencedirect.com

SCIENCE DIRECT

Thin Solid Films 484 (2005) 26–33

www.elsevier.com/locate/tsf

# Transparent conducting oxide thin films of $Cd_2SnO_4$ prepared by RF magnetron co-sputtering of the constituent binary oxides

Robert Mamazza Jr., Don L. Morel, Christos S. Ferekides*

*Department of Electrical Engineering, University of South Florida, 4202 East Fowler Avenue, Tampa, Fl 33620, USA*

Received 18 December 2002; accepted in revised form 20 January 2005
Available online 19 March 2005

**Abstract**

Thin films of cadmium tin oxide ($Cd_2SnO_4$) have been deposited on glass substrates by RF magnetron co-sputtering from cadmium oxide (CdO) and tin oxide ($SnO_2$) targets in an Argon ambient. Co-sputtering offers a means to control the atomic stoichiometry of $Cd_2SnO_4$, which influences the material's electro-optical and structural properties. The $Cd_2SnO_4$ films were deposited at room temperature and subsequently subjected to a heat treatment in inert or reducing ($H_2$) ambient. The as-deposited films were amorphous, and became polycrystalline after annealing at high temperatures. Using this method, $Cd_2SnO_4$ films with a Hall mobility of 32.3 $cm^2\ V^{-1}\ s^{-1}$ and a carrier concentration of $7.40\times10^{20}$ $cm^{-3}$ corresponding to a resistivity of $2.07\times10^{-4}$ Ω cm have been prepared. The films exhibited average optical total transmission in excess of 90% in the visible region. The optical bandgap was found to be in the range of 2.97–3.18 eV, depending on post deposition treatment.


*Keywords:* Cadmium stannate; Optical coatings; Oxides; Sputtering

## 1. Introduction

Transparent conducting oxides (TCOs) are both transparent to various wavelengths of light and conductive to electric current. Depending on the application, one or both of these properties must be optimized. Applications for TCOs include, but are not limited to, photovoltaic devices, flat panel displays (liquid crystal displays, LCDs) [1], gas sensors, architectural windows (window tint), and window deicing elements. The broad spectrum of applications of TCOs goes beyond what is mentioned here. Nevertheless, their significance is clearly evident. Applications in photovoltaics may place the highest demand on TCOs through their demand for the highest possible levels of optical transmission and electrical conductivity. Thin film solar cells require at least one of the contacts, typically the front, to be transparent.

At present tin oxide ($SnO_2$), indium tin oxide ($In_2O_3$:Sn or ITO), and zinc oxide (ZnO) are among the most prevalent materials employed as TCOs for thin film solar cell applications. In a transparent conducting oxide, the conductivity complements the optical transmission: the higher conductivity is beneficial because it affords the ability of manufacturing thinner films, which further increases the material's optical transmission; this assertion neglects IR reflection and absorption that can exist at longer wavelengths [2,3]. For many applications that place much of their concern on the visible portion of the spectrum, the above assertion can be justified.

Many single metal oxides ($SnO_2$, ZnO, and $In_2O_3$:Sn) have been thoroughly investigated and employed in many applications. As a result, most of their advantages and disadvantages are known. In order to make further advancements in TCOs, one must investigate new materials. Mixed metal oxides of the above-mentioned TCOs offer a solid starting point, as the materials are readily available and understood in terms of processing requirements and feasible outcomes. Examples of such endeavors have received

* Corresponding author.
*E-mail address:* ferekide@eng.usf.edu (C.S. Ferekides).

0040-6090/$ - see front matter © 2005 Elsevier B.V. All rights reserved.
doi:10.1016/j.tsf.2005.01.097

considerable attention of recent, and include, but are not limited to, materials such as $CdIn_2O_4$ [4], $Zn_2SnO_4$ [1,5], $ZnGa_2O_4$ [6,7], and $Cd_2SnO_4$ [8]. Of these, $Cd_2SnO_4$ has shown much promise for the preparation of highly conductive and transparent thin films. $Cd_2SnO_4$ was first investigated by Nozik in 1972 [9]. Haacke further investigated $Cd_2SnO_4$ and was one of the first to produce highly conductive films [3,10]. More recently, the National Renewable Energy Laboratory of the United States of America has reinforced the claims of those prior and further advanced the technology and understanding of this material [8]. Despite the success of these investigations – and others that followed – $Cd_2SnO_4$ has not been employed to any appreciable extent, commercially or otherwise.

Thermodynamically, $Cd_2SnO_4$ acquires a lower energy state when it crystallizes in the orthorhombic structure; however, sputtered films assume the inverse spinel structure [11,12]. Such phenomenon makes this material a unique compound and not a mere mixture of CdO and $SnO_2$. Consequently, the ratio of Cd and Sn cations becomes important for obtaining a homogeneous film without secondary phases such as CdO, $SnO_2$, or $CdSnO_3$. The spinel structure of Fig. 1, can be thought of in terms of the generic formula $(M^{2+})_2M^{4+}(O^{2-})_4$. For the present discussion, $M^{2+}$ shall be Cd, as it has an oxidation state of 2+ and $M^{4+}$ represents Sn. In the spinel structure, the anions ($O^{2-}$) are arranged in a cubic close packing (ccp) array, which forms both octahedral and tetrahedral holes. Of the available octahedral holes, the $M^{4+}$ ($Sn^{4+}$) cations are located in one half of these holes; the other half are occupied by $M^{2+}$ cations ($Cd^{2+}$) All of the available tetrahedral holes are occupied by the $M^{2+}$ cations ($Cd^{2+}$) [13]. In $Cd_2SnO_4$, it has been suggested that reduced $M^{2+}$ interstitials form *n-type* defects, contributing to conductivity [14]. Additionally, oxygen vacancies have also been proposed to contribute to the conductivity through the creation of a free electron orbital, i.e. one not involved in the formation of a bond [15]. However, it has been theoretically predicted that neither of the aforementioned defects are likely to account for the high number of free electrons that lead to highly conductive films of $Cd_2SnO_4$, for they have either too high formation energy or too high activation (or ionization) energy. Further, the suggested defect primarily responsible for the *n*-type conductivity of $Cd_2SnO_4$ is the substitution of an octahedrally coordinated Cd site by a $Sn^{4+}$ cation [13]. The purpose of this work was to investigate compositional (Cd to Sn ratio) effects on the eletro-optical and structural properties of $Cd_2SnO_4$, a TCO that may offer significant advantages over the commonly used binary oxides in advancing the efficiency and manufacturability of thin film solar cells.

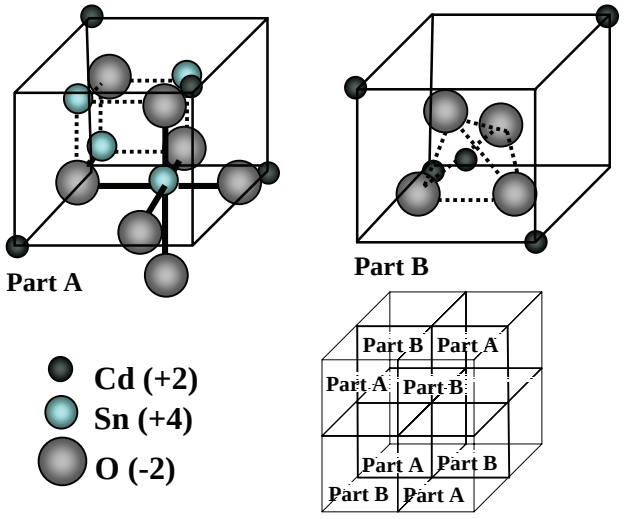


Fig. 1. Cubic spinel structure of $Cd_2SnO_4$. Each cubic face of either part is joined to the other part type, i.e. each part A is joined to six part B's at its cube's faces.

## 2. Experimental details

Cadmium stannate films were prepared by RF magnetron co-sputtering from CdO (99.99% pure assay) and $SnO_2$ (99.99% pure assay) targets at room temperature. The substrates used were Corning 7059 glass of dimensions $1.25\times1.45\times0.032$ in. Prior to deposition the substrates were cleaned using a 10% by volume solution of hydrofluoric acid followed by a rinse in deionized water. The magnetron sputtering sources were 3 in. diameter Kurt J. Lesker Taurus TRS3FSA models; Advanced Energy RFX-600 power supplies supplied the RF power. The sputtering sources were positioned such that the center axis was aligned with the center of the substrate holder forming an angle of approximately 22.5° with respect to a line orthogonal to the substrate holder. This geometry resulted in a source to substrate distance of approximately 10 cm. The sputter ambient was 100% Argon where the pressure was maintained at $3.0\pm0.1$ mtorr, which was monitored with an MKS Baratron® model PDR-D-1 absolute pressure transducer. The power density for each sputtering source was kept under 2.6 W/cm$^2$. The Cd to Sn ratios were changed through a tooling feature on the thickness monitors, which in effect manipulated the power to each gun. Annealing experiments were carried out in a simple evacuated closed end tube furnace with a stationary ambient of either He or $H_2$. The substrates were placed between two SiC coated graphite plates that were held apart by 2.5 mm quartz spacers. Both of the SiC coated graphite plates were heated by 2000-W tungsten halogen lamps (from the top and bottom). The temperature was determined by use of a thermocouple. Annealing temperatures ranged from 100 to 700 °C. For both ambient gases, He and $H_2$, the pressure at room temperature was approximately 500 torr. Anneal durations were typically 20 min. The film properties were characterized by XRD, SEM, AFM, energy dispersive spectroscopy (EDS), optical transmission spectroscopy, four-point-probe, and Hall Effect measurements.

Crystallinity and phase composition were determined using powder XRD. The diffractometer was a Miniflex (VD01417) manufactured by Rigaku with CuKá radiation ($\gamma$=1.540562 nm). The grain size was estimated using Sherer's equation,

$$D = \frac{0.9\lambda}{\beta \cos\theta} \tag{1}$$

where $D$ is the grain size; 0.9 is a constant; $\lambda$ is the wavelength; $\beta$ is the FWHM for the crystal direction in question (after correction for any instrumental peak broadening by use of a Si standard.); and $\theta$ is the Bragg angle[16]. Surface topography was elucidated using a Hitachi 800 SEM and a Scanning Probe Microscope Digital Instruments Nanoscope Dimension 3000 Atomic Force Microscope (AFM). The mean surface roughness, $R_a$, as determined using the AFM, was calculated by the following equation

$$R_a = \frac{1}{L_x L_y} \int_0^{L_y} \int_0^{L_x} |f(x,y)| \mathrm{d}x\mathrm{d}y \tag{2}$$

where $L_y$ and $L_x$ are the surface dimensions, and $f(x,y)$ is the function that represents the surface relative to the center plane. Molecular atomic composition, or stoichiometry, was determined through EDS analysis using a Tacor Northern (TN) 550 Energy dispersive Spectrometer in conjunction with a JOEL JSM 840 Scanning Electron Microscope. The accelerating voltage for the electron beam was 10 kV. This value was used to limit the electron beam's penetration into the substrate, which decrease the signal to noise ratio. The precision of the measurement was checked against $Cd_2SnO_4$ powder purchased from Fischer Scientific. Using five data points taken from various areas of the powder sample resulted in a variance of $\pm$0.035%. Subsequent measurements of $Cd_2SnO_4$ films were based on averages taken from at least 5 different areas of the film. A Tencor Alpha-step 200 profilometer was used for film thickness determination. A portion of the film was etched through to the substrate using hydrochloric acid and zinc powder. The prominent thickness investigated and presented herein was 2000$\pm$100 Å. For optical measurements, an Oriel Cornerstone model 74100 monochromator with an integrating sphere was utilized. The direct bandgap determination was based on the extrapolated linear regression of the curve resulting from a plot of photon energy versus the square of the absorption coefficient. The absorption coefficient was calculated according to the equation

$$\alpha = \left(\frac{1}{t}\right) \ln\left(\frac{1}{T}\right) \tag{3}$$

where $t$ is the film's thickness, and $T$ is the transmission at the wavelength in question [17]. Eq. (3) assumes the reflection in the short (high energy) wavelength region to be negligible. A more complete expression for the absorption coefficient is provided by Eq. (4)

$$\alpha = \left(\frac{1}{t}\right) \ln\left[\frac{(1-R)^2 + \sqrt{(1-R)^4 + (2RT)^2}}{2T}\right], \tag{4}$$

where $R$ is the reflection. Simply taking all of the $R$'s to be zero simplifies Eq. (4) into Eq. (3). It is shown in the literature that the reflectance of $Cd_2SnO_4$ in the 300–400 nm range is approximately 10% [8]. Inclusion of an $R$ value of 0.10 increased the calculated bandgap by less than 0.05 eV. As reflection measurements were not available at the time of the optical measurements, Eq. (3) was used to approximate values of the optical bang gap. Four-point probe measurements were used for sheet resistance and as quick means for resistivity approximations. Hall mobilities and carrier concentrations were obtained using the van der Pauw Method (a rectangular four-point probe arrangement) and a Keithley 920 Series Hall Test Equipment set-up. All of the reported resistivity values were acquired by Hall measurements.

## 3. Results and discussion

### 3.1. Film growth and crystallinity

$Cd_2SnO_4$ films were deposited at room temperature and subsequently subjected to a heat treatment under various conditions. It has been previously reported, that as-deposited, amorphous films become polycrystalline after annealing at temperatures above 580 °C [5]. Films prepared in this work were found to begin to crystallize at approximately 525 °C, as was confirmed by X-ray diffraction measurements. Fig. 2 displays the XRD spectra of various films annealed at temperatures ranging from 500 to 550 °C; an as-deposited sample (room temperature) is also included for comparison. At 525 °C the peak for the crystal plane perpendicular to the [222] direction appears; from these spectra, it is clear that the films exhibit preferential orientation along the [222] direction. This is in contrast to others' findings that have reported to have preferred orientations corresponding to the [311] direction [8]. This difference may be due to differences in the deposition process. The $Cd_2SnO_4$ films that exhibited preferred orientation in the [311] direction were prepared from a 33% $SnO_2$ 67% CdO composite target in pure oxygen at a pressure somewhere between 10 and 17.5 mtorr, and subsequently annealed in a CdS environment. The presence of oxygen in the film growth environment and the CdS in the anneal environment, may have had a thermodynamic or kinetic effect in the crystallization process leading to the above mentioned differences in the crystallographic orientation. In addition, differences in pressure and ambient ($O_2$ vs. Ar), would change the dynamics of the sputter

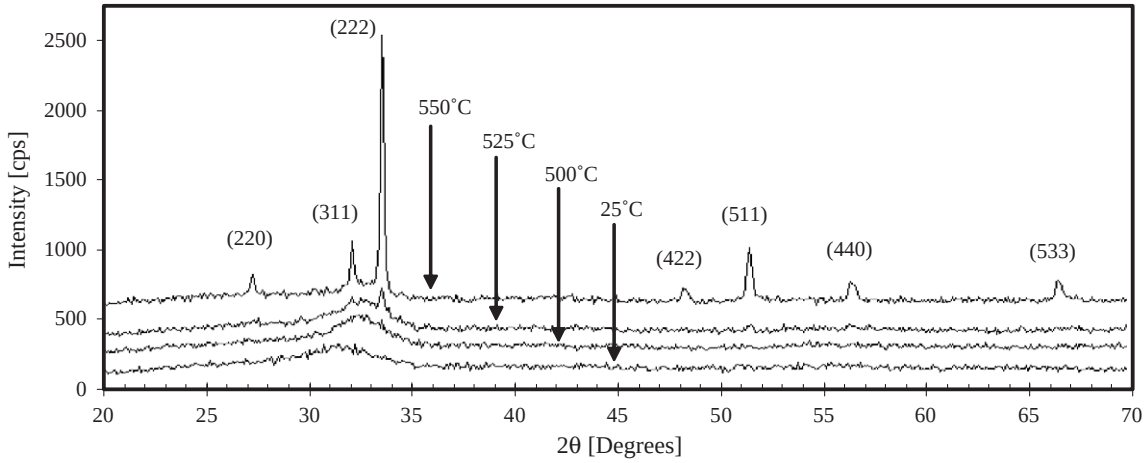


Fig. 2. XRD patterns for $Cd_2SnO_4$ films annealed at temperatures ranging from 500 to 550 °C.

process, including the deposition rate, further influencing the film orientation.

Films were annealed in He at temperatures above that required to initiate crystallization to determine the stability of these films at high temperatures. The films maintained homogeneity (i.e. no secondary phases of $SnO_2$, CdO, nor $CdSnO_3$) through temperatures to nearly 700 °C. At 700 °C, a secondary phase of $SnO_2$ appeared, as was indicated by the peak resulting from the reflection from the plane associated with the Miller indices of (110) (Fig. 3).

From the X-ray diffraction data, the grain size of various orientations at the various annealing temperatures was calculated using Eq. (1). These data are displayed in Fig. 4. For the [311] and the [511] crystal directions, the trend with temperature is nearly identical. However, for the crystallites with the [222] direction the relative trend is different, and almost opposite of the other two. The largest grains formed were approximately 78 nm, which corresponded to the [311] direction at a temperature of 550 °C. The second largest was approximately 73 nm for the [222] direction at 600 °C. The resistivities for films annealed at both these temperatures were nearly identical. At higher temperatures, the resistivities began to increase (see Fig. 7). At 700 °C, the crystal size of all directions began to decrease. From Fig. 3, it can be seen that the material begins to decompose, as was indicated by the formation of a secondary phase of $SnO_2$. The effect of the heat treatments on the electrical and optical properties of the $Cd_2SnO_4$ films will be discussed in subsequent sections.

### 3.2. Surface topography

It has been previously stated that one of the advantages of $Cd_2SnO_4$ is that it has superior surface properties in terms of its relative smoothness (or low roughness) compared to other TCOs, namely $SnO_2$ [1]. Fig. 5 depicts AFM micrographs of $Cd_2SnO_4$ films: the top image is of an as-deposited at room temperature sample which is amorphous, and the bottom image is for the same sample after annealing at 600 °C in He for 20 min, which caused it to crystallize. X.

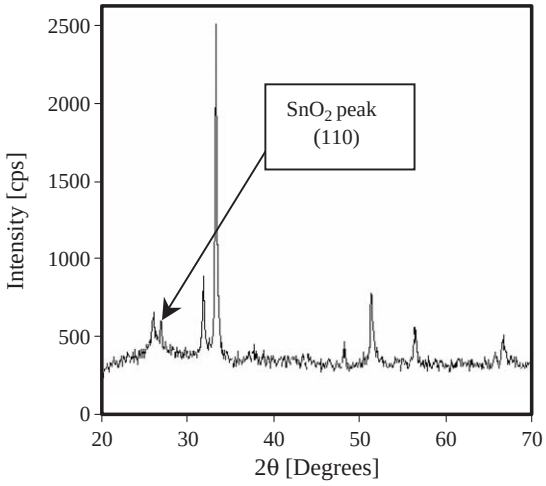


Fig. 3. XRD pattern for $Cd_2SnO_4$ annealed at 700 °C showing the appearance of a $SnO_2$ phase.

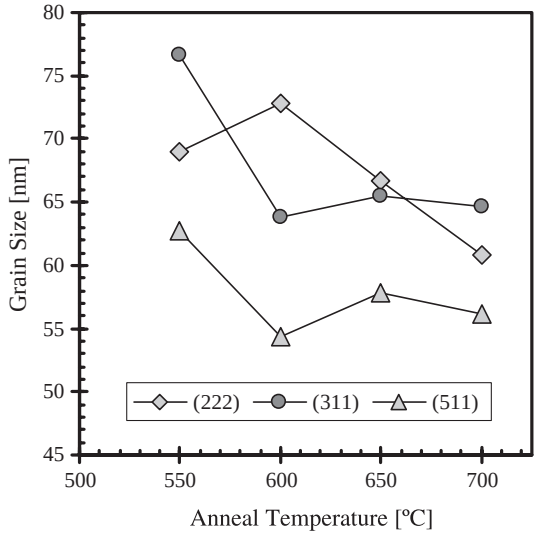


Fig. 4. Crystal size as a function of film anneal temperature for the (222), (311), and (511) diffraction peaks.

Wu et al. have reported a mean (average) surface roughness, $R_a$, value, determined by AFM, of 1.3 nm for polycrystalline $Cd_2SnO_4$ coatings [5]. The value determined in this work, for the polycrystalline film in Fig 5, was 1.4 nm, which is consistent with the aforementioned value. The as deposited (amorphous) films were considerably smoother, with a mean roughness value of 0.39 nm. It can be seen from the scale bar that the width of an individual grain (Fig. 5—bottom; polycrystalline film) is roughly 70 nm, which is consistent with the average grain size determined by XRD.

### 3.3. Stoichiometry and resistivity

It has been previously suggested that a slight excess in Cd leads to an increase in the number of Cd interstitials, which will in turn lower the material's resistivity [10]. The atomic ratio of Cd to Sn was varied around the stoichiometric ratio of 2.0, by varying the sputtering power applied to one of the sources while the other was held constant. The films were grown to a thickness of 2000 Å. All films were annealed at 600 °C in He (the 600 °C anneal temperature was selected based on data presented in Section 3.4). Fig. 6 displays the resistivity as a function of the Cd to Sn ratio for values of 1.5 to 2.4. The Cd to Sn ratio was calculated

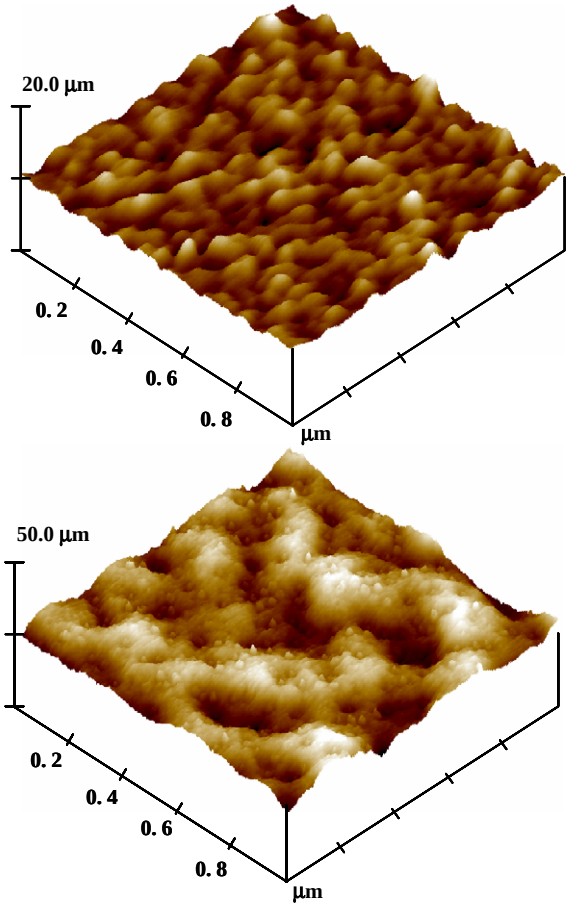


Fig. 5. AFM micrographs of the surface of $Cd_2SnO_4$; top—as deposited; bottom—annealed at 600 °C in He.

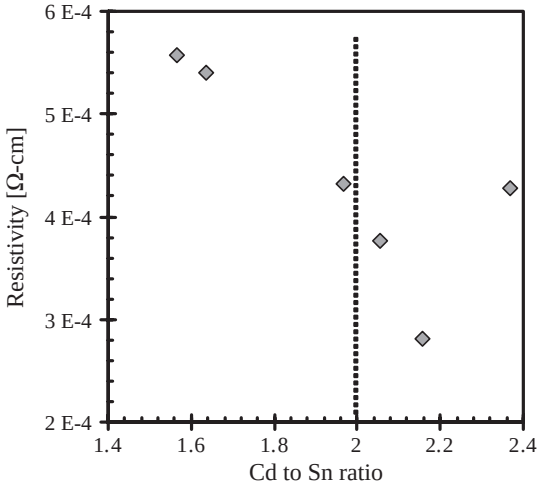


Fig. 6. Dependence of resistivity on the Cd to Sn ratio (measured by EDS).

from EDS measurements. The ratio was calculated after averaging the atomic concentrations measured at least at 5 different areas of the $Cd_2SnO_4$ films. It can be seen that an excess (estimated to be about 7% higher than a 2:1 ratio) of Cd produced the lowest resistivity while at lower or higher ratios the resistivity appears to exhibit a rather sharp increase. The resistivity for the optimum Cd to Sn ratio of 2.15 was found to be $2.6\times10^{-4}$ Ω cm. The excess Cd, within the range where the spinel phase can form without secondary phases of $SnO_2$ and CdO, is said to produce Sn-rich environment through the codependent nature of the chemical potentials, $\mu_{Cd}$ and $\mu_{Sn}$, of the Cd and the Sn, as proposed by Zhang and Wei [13]. Accordingly, under a Sn rich environment, the probability of a Sn on a Cd site increases. When this Sn occupies a Cd octahedral site, it acts as a donor, which explains the decreased resistivities of films grown under Cd-rich environment. The increase in resistivity at lower Cd to Sn ratios is a result of a lower carrier concentration (see Fig. 11), further supporting this claim.

### 3.4. Effect of annealing on resistivity

Upon determination of an optimum Cd to Sn ratio, the effect of the annealing temperature in an inert ambient (He) on resistivity was investigated. The films were deposited at a Cd to Sn ratio of 2.15 and subsequently annealed in the temperature range of 550 to 700 °C. Lower annealing temperatures were not investigated since the films remained amorphous at temperatures below 550 °C. In all instances the resistivity was lowered upon annealing. The lowest resistivity values were obtained for annealing temperatures in the 550 to 600 °C range. It was determined that the resistivity of $Cd_2SnO_4$ remains relatively constant up to 600 °C, and it begins to increase at higher temperatures. Fig. 7 shows these changes in resistivity as a percent difference from the initial value (the value of the as deposited amorphous film). The greater the percent, the greater was

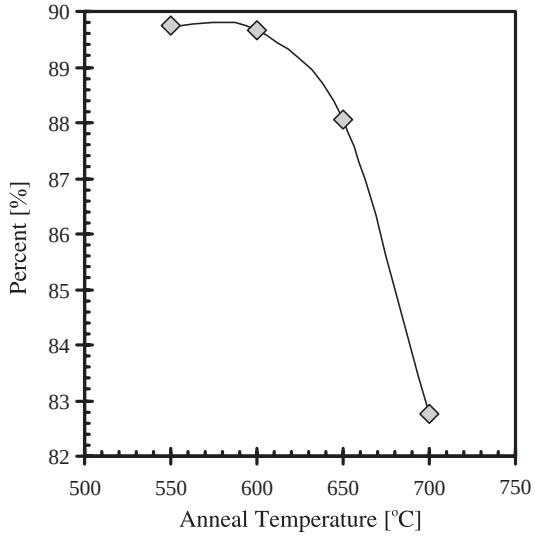


Fig. 7. Percent difference of resistivity as a function of anneal temperature (He ambient).

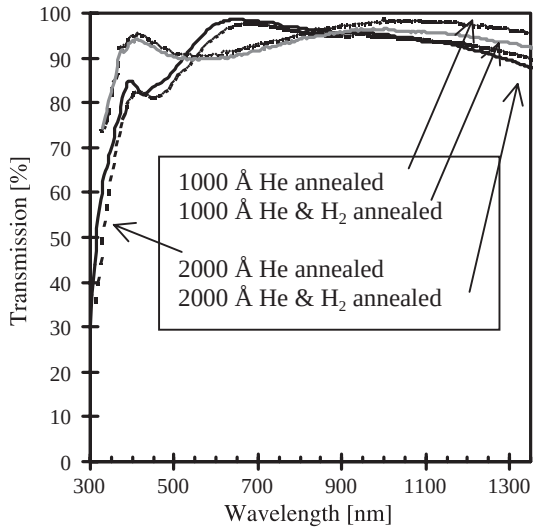


Fig. 8. Total transmission for $Cd_2SnO_4$ films of 1000 and 2000 Å with different post deposition treatments: He only and He followed by $H_2$.

the change in resistivity. At 700 °C, the resistivity, though lower than the as-deposited film, was the highest among all annealed films. This can be partly attributed to the formation of a secondary phase of $SnO_2$ as seen in the XRD pattern in Fig. 3. This $SnO_2$ may be described as intrinsic. It is even plausible to assume it to be Cd-doped, which would make it even more resistive. At 650 °C, it may be due to changes in the crystal structure, as was indicated by the changing grain sizes at these temperatures.

Films annealed at 600 °C were subsequently annealed in $H_2$ to determine the effects of a reducing environment. It was determined that 400 °C was the upper limit of the film's integrity in a $H_2$ environment, and consequently this was the temperature used for subsequent treatments. At temperatures above 400 °C, the films began to decompose, as was evident by the formation of a gray haze about the surface. Further, slight optical and electrical effects were resultant from the $H_2$ anneals at 400 °C. Lower temperatures yielded little or no change in these properties. These effects are discussed in the following two sections.

### 3.5. Optical transmission

The optical transmission of annealed 1000 and 2000 Å thick $Cd_2SnO_4$ films is shown in Fig. 8. The annealing ambients used for these films were He and $H_2$. The average transmission for the 1000 and 2000 Å samples was in excess of 90% in the range of 400 and 1000 nm. For the same two samples small differences between the two annealing ambients were observed in the 350 to 450 nm range. Above 650 nm, a slight loss in transmission (<3%) resulted from the $H_2$ annealing, which can be attributed to free carrier reflection/absorption resulting from the higher carrier concentration in this film (see Table 1). It is also observed that this result is less pronounced for thicker films. This is believed to have resulted from the kinetics of the reaction process of the $H_2$ with the $Cd_2SnO_4$. The extent of this chemical reaction will be less with the thicker film for the same time duration. Transmission losses at longer wavelengths result from photon–electron interaction, which can scatter the photons. Losses occur from both reflection and absorption. It is beneficial to state that the reflection in this region is not strictly a surface phenomenon. Reflection from the bulk of the material can also occur, provided that the electron escapes the surface. If the scattered electron does not escape the surface, it can be concluded to have been absorbed. As the reflectance was not measured, the specific mechanism behind the loss of transmission (either reflection or absorption) cannot be definitively stated. For the 350 to 450 nm wavelength region the effect of the $H_2$ anneal manifested itself in the form of a shift (shown in Fig. 9). This shift was greatest for the 2000 Å sample, approximately 11 nm, resulting in an apparent increase of 0.21 eV in the bandgap of $Cd_2SnO_4$. It is assumed that this shift of the absorption edge towards shorter wavelengths (higher energy) resulted from the increase in carrier concentration in accordance with the Moss–Burstein effect. For the 1000 Å sample no such a shift is observed; the reason for this is not fully understood, but it is believed that surface scattering effects may begin to dominate due to the reduced bulk thickness. These effects may interfere with the Moss–Burstein effect.

Table 1
Summary of He only and He followed by $H_2$ annealing on $Cd_2SnO_4$ and the effect on electron mobility, carrier concentration, resistivity, and band gap for 2000 Å samples

| Conditions | Mobility [$cm^2\ V^{-1}\ s^{-1}$] | Carrier concentration [$cm^{-3}$] | Resistivity [Ω cm] | Band gap [eV] |
|---|---|---|---|---|
| 600 °C He | 32.3 | $7.4\times10^{20}$ | $2.07\times10^{-4}$ | 2.97 |
| 600 °C He/ 400 °C $H_2$ | 29.2 | $8.5\times10^{20}$ | $2.01\times10^{-4}$ | 3.15 |

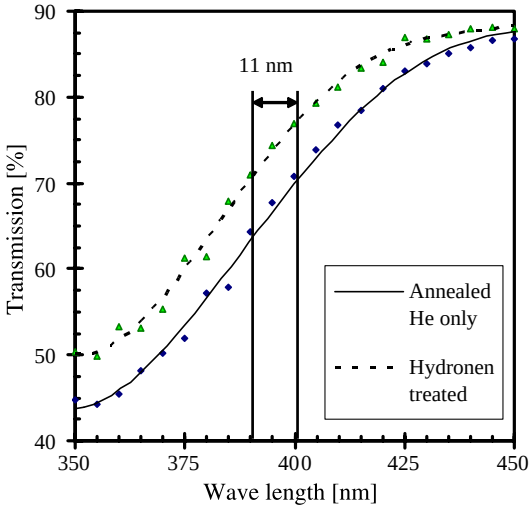


Fig. 9. Close-up of the curve shift in Fig. 8 for the 2000 Å thick sample resulting from the $H_2$ anneal.

Direct band-to-band transition energies were also determined from the transmission data for the 2000 Å thick sample (see Fig. 10). The bandgap of $Cd_2SnO_4$ was determined to be approximately 2.97 eV, which is within the range of values reported in the literature surveyed (2.7–3.0 eV) [8,13,14]. The $H_2$ annealing, as described above resulted in a slightly larger bandgap of 3.18 eV, which lies just outside the range of reported values. Higher electron energy band to band transitions result from high doping concentrations that introduce a sufficient number of states as to shift the Fermi level into the conduction band. To some finite point, the Fermi level can be shifted to higher values by further increasing the doping level. It is seen from the carrier concentration data that the sample annealed had the highest carrier concentration and accordingly the larger bandgap. The upper limit of this effect was not studied.

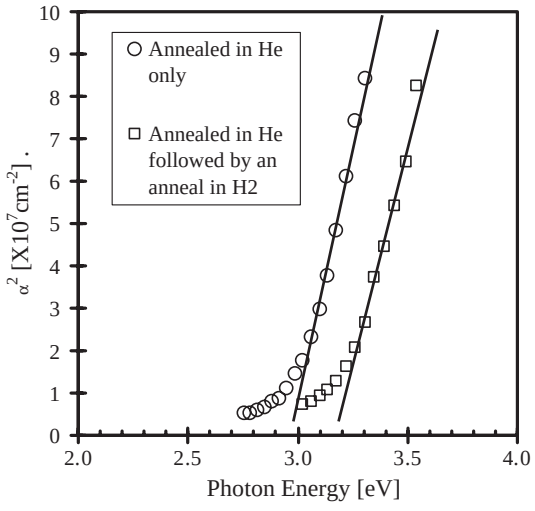


Fig. 10. Direct optical band-to-band transition energy for $Cd_2SnO_4$ annealed in He only and He followed by $H_2$.

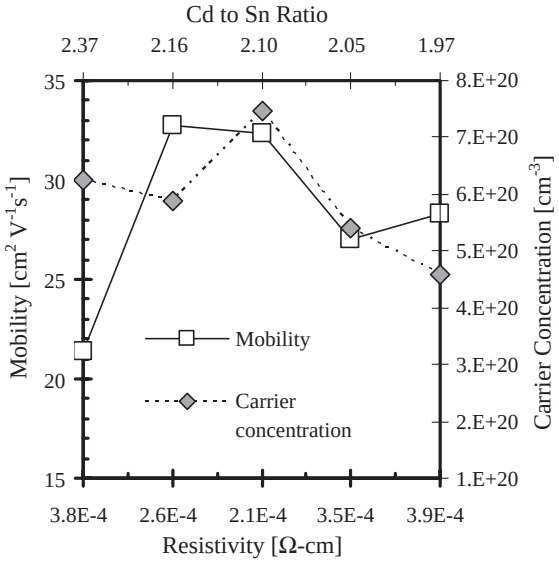


Fig. 11. Mobility, carrier concentration, and resistivity as a function of the Cd to Sn ratio for 2000 Å thick films.

### 3.6. Mobility and carrier concentration

The mobility and carrier concentration were investigated as a function of the Cd to Sn ratio for annealed $Cd_2SnO_4$ films (see Fig. 11). In support of the results produced in Fig. 6, the highest value of carrier concentration ($7.4\times10^{20}$ $cm^{-3}$) and the second highest mobility (32.3 $cm^2$ $V^{-1}$ $s^{-1}$) were obtained for films deposited at excess Cd conditions. These data are in agreement with previous claims that slight excess Cd can lead to an increase in the number of Sn octahedral sites, which in turn will increase the number of charge carriers [13]. The increase in resistivity at Cd to Sn ratios above approximately 2.16 was primarily from a drop in mobility. For samples with a Cd/Sn ratio of less than 2.10, the carrier concentration's decline was the reason for the observed increase in resistivity. $Cd_2SnO4$ films subsequently annealed in $H_2$ displayed a small drop in mobility (29.2 $cm^2$ $V^{-1}$ $s^{-1}$) but an increase in carrier concentration ($8.47\times10^{20}$ $cm^{-3}$). This is believed to result from the reduction on oxygen sites in the lattice creating oxygen vacancies. These oxygen vacancies are defects that can decrease an electron's mobility by increasing the number of scattering sites within the lattice.

## 4. Conclusion

$Cd_2SnO_4$ films with varying Cd to Sn ratios were deposited by co-sputtering CdO and $SnO_2$. The as-deposited films were found to be amorphous and were subjected to heat treatments under various conditions (He and $H_2$ at different temperatures) in order to improve their structural properties. It was determined that the films began to crystallize at approximately 550 °C; decomposition through a secondary phase of $SnO_2$ began at approximately 700 °C.

Films with excess Cd produced the lowest resistivities. Such films exhibited the highest charge carrier densities of $7.40\times10^{20}$ $cm^{-3}$ with the highest Hall mobility being 32.3 $cm^2$ $V^{-1}$ $s^{-1}$. Subsequent annealing in $H_2$ marginally improved the material's resistivity by approximately 3.0%. The benefit, however, resulted from the higher carrier density of $8.47\times10^{20}$ $cm^{-3}$ (an increase of approximately 15%). This higher carrier density increased the optical bang gap of $Cd_2SnO_4$ from 2.97 to 3.18 eV, a difference of approximately 0.2 eV, which ranks among the higher values found in the literature surveyed. The co-sputtering process used in this work produced $Cd_2SnO_4$ thin films with resistivities as low as $2.01\times10^{-4}$ Ω cm, sheet resistances of approximately 10.0 Ω/□ (for 2000 Å thin films), average optical transmission (between 400 and 900 nm) in excess of 90%, and Hall mobilities and carrier concentrations as high as 32.3 $cm^2$ $V^{-1}$ $s^{-1}$ and $7.40\times10^{20}$ $cm^{-3}$, respectively.

## Acknowledgements

This work was supported by the New Energy and Industrial technology Development Organization (NEDO) of Japan and the National Renewable Energy Laboratory. The authors would like to thank Jeff Rian and Paul Bryan from the department of Geology at the University of South Florida for the use of their X-ray diffractometer, and acknowledge the Nanomaterials and Nanomanufacturing Research Center for the use of Atomic Force and Scanning Electron Microscopes.

## References

[1] T.J. Coutts, D.L. Young, X. Li, W.P. Mulligan, X. Wu, J. Vac. Sci. Technol., A, Vac. Surf. Films 18 (6) (2000) 2646.
[2] K.L. Chopra, S. Major, D.K. Pandya, Thin Solid Films 102 (1) (1983) 1.
[3] G. Haacke, H. Andro, W.E. Mealmaker, Solid State Sci. Technol. 124 (1977) 1923.
[4] R. Mamazza, U. Balasubramanian, D.L. Morel, C.S. Ferekides, in: T. Jester, H. Ullal, D. Marvin, J. Yang, J. Wohlgemuth (Eds.), Proceedings of the 29th IEEE Photovoltaic Specialists Conference, New Orleans, U.S.A., May 20–24, 2002, p. 612.
[5] X. Wu, S. Asher, D.H. Levi, D.E. King, Y. Yan, T.A. Gessert, P. Sheldon, J. Appl. Phys. 89 (2001) 4564.
[6] R. Pandry, J.D. Gale, S.K. Sampath, J.M. Recio, J. Am. Ceram. Soc. 82 (12) (1999) 3337.
[7] Z. Yan, H. Takei, J. Cryst. Growth 171 (1997) 131.
[8] X. Wu, W.P. Mulligan, T.J. Coutts, Thin Solid Films 286 (1996) 274.
[9] A.J. Norzik, Phys. Rev., B 6 (1972) 453.
[10] G. Haacke, Appl. Phys. Lett. 28 (1976) 622.
[11] L.A. Siegel, J. Appl. Cryst. 11 (1978) 284.
[12] S.H. Wei, S.B. Zhang, Phys. Rev., B 63 (2001) 045112.
[13] S.B. Zhang, S. Wei, Appl. Phys. Lett. 80 (2002) 1376.
[14] Y. Dou, R.G. Egdell, Phys. Rev., B 53 (23) (1996) 15405.
[15] T. Stapinski, E. Leja, T. Pisarkiewitz, J. Phys., D Appl. Phys. 17 (1984) 407.
[16] E.M. Bachari, G. Baud, S. Ben Amor, M. Jacquet, Thin Solid Films 348 (1999) 165.
[17] F. Javier Yusta, M.L. Hitchman, S.H. Shamlian, J. Mater. Chem. 7 (8) (1997) 1421.